=====================MATHEMATICAL MODELING =====================

Polarons on Dimerized Lattice of Polyacetilene. Continuum Approximation

Astakhova T.Yu.*, Vinogradov G.A.**

Emanuel Institute of Biochemical Physics, Russ. Acad. Sci., Moscow, Russia

Abstract. A one-electron model is proposed to describe a polaron on a dimerized polyacetylene lattice. Within the framework of the formulated model, the dynamics of a freely moving polaron is considered. The results obtained are compared with the many-electron model that takes into account all π-electrons of the valence band. Polaron can move at subsonic and supersonic speeds. The subsonic polaron is stable. A supersonic polaron loses stability at times $\sim 6\,000$ fs. A supersonic polaron has a forbidden speed range. An analytical solution to the continual approximation helps to understand the reason for the existence of forbidden speeds. The dynamics of a free polaron is similar to the dynamics of a polaron in an electric field. The proposed one-electron approximation significantly expands the possibilities of numerical simulation in comparison with the traditional many-electron model.

Key words: polaron, polyacetilene, continuum approximation, dimerized lattice.

INTRODUCTION

There is a large family of polymers with conjugated bonds, which, upon doping, transform from the state of wide-gap semiconductors to materials with a metallic type of conductivity. This discovery made it possible to use these polymers in solar energy cells, sensors, batteries and other applications [1, 2, 3]. The most famous and studied example of such polymers is polyacetylene (PA) [4, 5, 6]. Simultaneously with experimental studies aimed at obtaining practical results, the field of theoretical studies of low-dimensional many-electron systems was opened. And special attention has been focused on polyacetylene (PA).

At present, the polaron [7] is the main mechanism of charge transfer in PA. A polaron is formed when, upon doping with electron donors, the polymer chain acquires an extra electron. As a result of the electron-phonon interaction, a polaron is formed. In the presence of an electric field, a polaron is capable of transferring an electric charge.

The most famous approach used in the theory of conducting polymers is the Su-Schrieffer-Heeger (SSH) model [8, 9]. Note that the SSH Hamiltonian was "experimentally" confirmed [10]. The SSH model takes into account only π-electrons. The influence of σ-electrons is described using classical potentials. The PA σ-bones tend to equalize the bond lengths, as in polyethylene; the π-electrons, due to the exchange interaction, tend to decrease bond lengths. A compromise between these tendencies is achieved by lattice dimerization – the formation of single and double bonds differing in length. Dimerization is also the main reason for the formation of the band gap. Due to its clear physical meaning and simplicity, the model was also used to calculate other systems, in particular, DNA [11].

A large number of works [12, 13, 14, 15, 16, 17, 18, 19, 20, 21] are devoted to the numerical

---

*astakhova1967.t@yandex.ru
**gvin@deom.chph.ras.ru

simulation of charge transfer by the polaron paradigm using the SSH Hamiltonian. Special attention was paid to the dynamics of a polaron in an electric field. It is found that, depending on the electric field strength E, the stationary polaron speed can be subsonic, close to the speed of sound, or supersonic, exceeding the speed of sound by ≈ 3 times. In this case, there is such a critical value of the field strength E_{cr} that for $E < E_{cr}$ the polaron speed is subsonic, and for $E > E_{cr}$ the polaron becomes supersonic [16, 22, 20, 23, 24]. In this case, the speed jump occurs in a very narrow range of changes in the values of E. The motion of a polaron in an electric field was considered in other approximations [25, 26].

Several results have been left without proper explanation. First, why is it possible for the existence of supersonic quasiparticles (polarons) on a lattice with a harmonic potential; secondly, what is the mechanism that causes the stepwise nature of the speed change depending on the field strength; and third: a supersonic polaron has a forbidden speed range. These questions still remain unexplained.

One of the reasons for this is the extreme time consumption in numerical modelling, which did not allow a detailed study of stationary regimes. It was necessary to take into account all π-electrons occupying the valence band and the number of equations to be integrated is equal to $\sim N^2/2$, where N is the lattice size. However, the role of these π-electrons is reduced only to ensuring lattice dimerization; they do not affect the polaron dynamics in any way.

The problem with the "superfluous" integration of equations for π-electrons was solved when the one-electron (OE) model [27, 28] was proposed. In this model, lattice dimerization was provided by additional classical potentials, and a single electron occupied the lowest level of the conducting band. It was shown that the OE model fully reproduces all the main results of the previously used multielectron (ME) model.

In this work, the study of the OE model is continued. Compared to the previous work [28], a lattice with free boundary conditions is considered (cyclic boundary conditions preserve the full length of the lattice and the formation of a polaron leads to the appearance of additional stresses, which results in a change in the polaron dynamics at long times). A continual solution for a polaron is also obtained in this work. This solution helps to clarify the situation with the existence of the forbidden speed range for a supersonic polaron.

The next section describes the OE model and compares it with the ME model. The continual approximation and the results obtained are briefly described below. The details of the derivation of the continual equations and their solution are given in the Appendix.

ONE-ELECTRON MODEL OF POLYACETYLEN

The Hamiltonian of polyacetylene (PA) in the framework of the OE model is the sum of quantum and classical Hamiltonians:

$$H = H_{el} + H_{lat}, \tag{1}$$

where the quantum Hamiltonian in the SSH representation has the form:

$$H_{el} = -\sum_j [t_0 - \chi(x_{j+1} - x_j - r_{av})] \left[c_{j+1}^+ c_j^- \, F + \text{c.c.} \right]. \tag{2}$$

Here x_j is the absolute coordinate of the j-th lattice site (lattice site is the CH-group of PA); r_{av} – average distance between the lengths of single and double bonds; t_0 – hopping integral in equilibrium; χ – parameter of electron-phonon interaction; $c^{+/-}$ – creation/annihilation operators of an electron at the site j. F is a factor that ensures the interaction of the polaron charge with the electric field. This factor has the form: $F \equiv \exp\left(-i\dfrac{eEr_{av}}{\hbar}t\right)$, where $e, E -$

electron charge and electric field strength; $\bar{h}$ is the Dirac constant. Note that a more natural notation for the interaction of a field with a charge is the expression: $F' = (Ejr_{\text{av}}) \cdot (ec_j^+ c_j)$, where Ejr_{av} is the potential of the electric field at site j, and $ec_j^+ c_j$ is the charge density at site j. The gauge invariance of the vector potential allows one to transform one representation into another [29]. The representation F, where the time t appears instead of the spatial variable j, is more convenient in numerical calculations.

Classical lattice Hamiltonian has the form:

$$H_{\text{lat}} = \frac{K_{\text{s}}}{2} \sum_{j=1,N/2}^{(\text{single})} (x_{2j} - x_{2j-1} - r_{\text{s}})^2 + \frac{K_{\text{d}}}{2} \sum_{j=1,N/2}^{(\text{double})} (x_{2j+1} - x_{2j} - r_{\text{d}})^2 + \frac{M}{2} \sum_{j=1,N} \dot{x}_j^2, \quad (3)$$

where $K_{\text{s}}, K_{\text{d}}$ – bond rigidities between lattice sites of single (s) and double (d) bonds. Summation in (3) runs separately over these bonds; M – mass of CH group. Equilibrium bond lengths are $r_{\text{s}} = r_{\text{av}} + \delta$ and $r_{\text{d}} = r_{\text{av}} - \delta$, where $\delta = (K_{\text{d}} - K_{\text{s}})/(K_{\text{d}} + K_{\text{s}})$ – alternation parameter for bond lengths.

The following parameter values are used: $t_0 = 2.5\,\text{eV}$; $\chi = 6.0\,\text{eV/Å}$; $r_{\text{av}} = 1.22\,\text{Å}$; $K_{\text{s}} = 14.0\,\text{eV/Å}^2$; $K_{\text{d}} = 16.0\,\text{eV/Å}^2$; $M = 1349\,\text{eV fs}^2/\text{Å}^2$; $\delta \approx 0.0813\,\text{Å}$. The sound speed is $v_{\text{snd}} = \sqrt{\dfrac{K_s^2 + K_d^2}{(K_s + K_d)M}}\, r_{\text{av}} \approx 0.13\,\text{Å/fs}$.

When an extra electron is placed on the PA lattice, a polaron is formed, and the next problem is to find a solution for a stationary polaron on the lattice. This solution will be used as an initial condition for studying subsequent dynamics. The solution is sought using an iterative procedure to find the coordinates of the lattice sites and the polaron wave function. This procedure is implemented as follows. Some "trial" coordinates of the x_j sites are fetched. These values are used to fill the $G(N \times N)$ matrix of the Hamiltonian (2). Matrix elements on side diagonals:

$$G(j, j+1) = -[t_0(x_{j+1} - x_j - r_{\text{av}} \pm \delta)]; \quad G(j+1, j) = G(j, j+1), \quad (4)$$

where sign $'+'$ is used for odd values of j, and $'-'$ is used for even j. The matrix $\mathbf{G}$ is diagonalized. The new values of the coordinate differences are found from:

$$\begin{aligned}
(x_{2j} - x_{2j-1} - r_{\text{av}} - \delta) &= -\frac{2\chi}{K_{\text{s}}}\phi_{2j-1}\phi_{2j}; \\
(x_{2j+1} - x_{2j} - r_{\text{av}} + \delta) &= -\frac{2\chi}{K_{\text{d}}}\phi_{2j+1}\phi_{2j+1},
\end{aligned} \quad (5)$$

where $\{\phi^{\text{LUMO}}\}$ is the $(N/2+1)$-th eigenvector of the corresponding matrix (LUMO = Lowest Unoccupied Molecular Orbital). The left-hand sides of the equations (5) are substituted into the matrix of the Hamiltonian (2). The matrix is diagonalized again and the eigenvectors of this matrix $\{\phi^{\text{LUMO}}\}$ are found. The process is repeated until energy convergence is achieved. Thus, coordinates $\{\mathbf{x}\}$ of the lattice sites are found. Complex wave functions are obtained by replacing $\{\phi^{\text{LUMO}}\} \Rightarrow \{\Psi\}$.

Equations for the classical and quantum subsystems follow from the Hamiltonians (2) and (3). In this case, the classical equations are divided into two groups – for even and odd

sites:

$$\begin{aligned}
M\ddot{x}_{2j} &= -K_\text{s}(x_{2j} - x_{2j-1} - r_\text{s}) + K_\text{d}(x_{2j+1} - x_{2j} - r_\text{d}) + \\
&\quad + \chi[F(\Psi^*_{2j+1}\Psi_{2j} - \Psi^*_{2j-1}\Psi_{2j}) + \text{c.c.}]; \\
M\ddot{x}_{2j+1} &= -K_\text{d}(x_{2j+1} - x_{2j} - r_\text{d}) + K_\text{s}(x_{2j+2} - x_{2j+1} - r_\text{s}) + \\
&\quad + \chi[F(\Psi^*_{2j+2}\Psi_{2j+1} - \Psi^*_{2j}\Psi_{2j+1}) + \text{c.c.}].
\end{aligned} \tag{6}$$

Schrödinger's equation has the form:

$$i\overline{h}\dot{\Psi}_j = -[t_0 - \chi(x_{j+1} - x_j - r_\text{av})]F\Psi_{j+1} - [t_0 - \chi(x_j - x_{j-1} - r_\text{av})]F^*\Psi_{j-1} \tag{7}$$

For a graphical presentation of the results, it is convenient to enter renormalized distances between neghbouring sites z_j:

$$\begin{aligned}
z_{2j-1} &= x_{2j} - x_{2j-1} - r_\text{s}; \\
z_{2j} &= x_{2j+1} - x_{2j} - r_\text{d}.
\end{aligned} \tag{8}$$

These coordinates are convenient because their values differ from zero only in the polaron domain. In this area, single bonds become shorter and double bonds longer. The charge density distribution averaged over three sites has the form:

$$q_j = \left(|\Psi_{j-1}|^2 + 2|\Psi_j|^2 + |\Psi_{j+1}|^2\right). \tag{9}$$

Figure 1 shows the lattice distortions in the polaron region in the z-representation and the averaged charge for the OE model and, for comparison, the same for the well-known ME model.
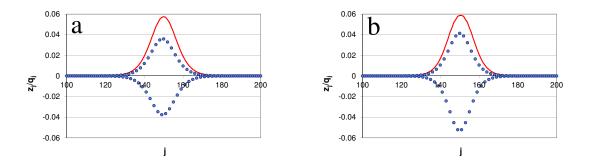

Fig. 1. Lattice distortions (solid circles) and averaged charge (solid line) for a stationary polaron for the ME model (**a**) and the OE model (**b**). $N = 300$.

The following figures shows a comparison of the polaron speeds in the ME and OE models in an applied electric field.

It follows from both figures that the proposed OE model qualitatively correctly describes the main features of a polaron on a dimerized lattice. A more careful selection of the parameters of the OE model can achieve a better agreement. However, the aim of this work is to analyze numerically and analytically the features of the dynamics of a freely moving polaron, when small deviations from the standard ME model are insignificant.
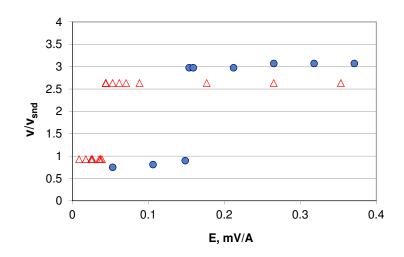
Fig. 2. Stationary polaron speeds (relative to the speed of sound) depending on the electric field strength for the ME model (circles) and the OE model (triangles). $N = 3\,000$.

Free-moving polaron

For the numerical simulation of a freely moving polaron, it is necessary to set the initial conditions: the coordinates and speeds of the lattice sites, as well as the wave function of the polaron. This can be done with an analytical solution. The details of obtaining the analytical solution are given in the Appendix, and here we will use these results to study the dynamics of a freely moving polaron.

The geometric profile of a polaron varies greatly with speed. Figure 3 shows the profiles of the lattice geometry deviations from equilibrium in the polaron region at different polaron speeds for the OE and ME models. Here the deviation from the equilibrium position is y_j:

$$y_j = x_j - x_j^0, \tag{10}$$

where x_j^0 is the coordinate of the site in the absence of a polaron, and x_j is the actual coordinate. The polaron profile strongly depends on whether the polaron is subsonic or supersonic. In the Appendix, two different solutions are obtained for these polarons.

Each of these panels has two dotted lines. Each of them refers to odd or even lattice sites. Bearing in mind that one of the goals of the work is to obtain an analytical solution, it is necessary to try to express the results obtained numerically in an analytical form. Figure 4 schematically shows an approximation of the deviations of the lattice y_j from equilibrium for the case shown in panel (f) of Figure 3. In the figure, the symbols represent the numerical values of y_j. The circles on the left are odd sites. For them, the approximating curve 5 is the sum of two contributions. The first is the hyperbolic tangent $A_1 \tanh(j + \Delta_{\text{lat}})$ (curve 1), the second is $A_2 / \cosh^2(j + \Delta_{\text{lat}})$ (curve 3). The resulting curve 5 is the sum of these two curves. The coincidence of the numerical values with their approximation is quite good. The same thing happens for even sites. Curve 6 is the sum of curves 2 ($A_1 \tanh(j - \Delta_{\text{lat}})$) and 4 ($A_2 / \cosh^2(j - \Delta_{\text{lat}})$). The value $2\Delta_{\text{lat}}$ is the distance between tangential approximations for even and odd sites. Such an approximation
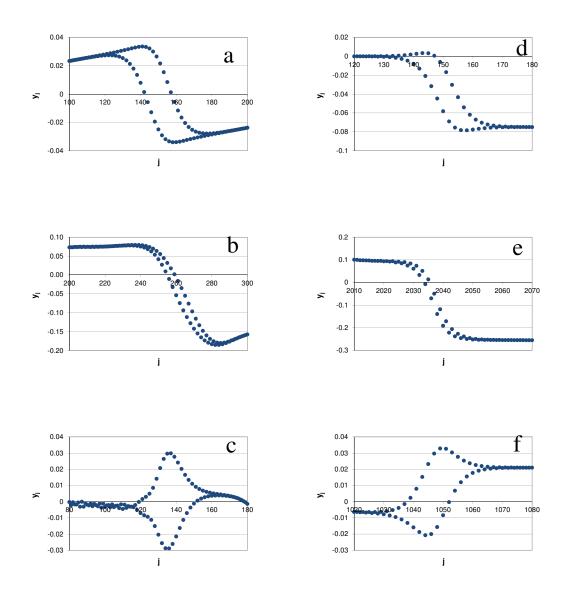
339

Fig. 3. Deviations from equilibrium positions for polarons moving at different speeds for the ME model (3 left panels) and the OE model (3 right panels). Polaron speeds are measured in units of the speed of sound: $v_p = 0$ (**a**), $v_p = 0.98$ (**b**), $v_p = 2.9$ (**c**); $v_p = 0$ (**d**), $v_p = 0.94$ (**e**); $v_p = 2.5$ (**f**).

makes it possible to search for an analytical solution in components in the general form:

$$
\begin{aligned}
p(\xi, t) &= A_1 \tanh\left[d(\xi - v_p t)\right]; \\
q(\xi, t) &= \frac{A_2}{\cosh^2\left[d(\xi - v_p t)\right]},
\end{aligned}
\tag{11}
$$

where the discrete coordinate j corresponds to the continual ξ: $j r_{av} \Rightarrow \xi$; d is the parameter of the width in the continuum approximations.

It is also convenient to split the wave function into two parts. One part is localized at odd sites, the other at even ones (Fig. 5). Here the signs of the wave function are the same for neighboring odd-even sites and alternate at even-even and odd-odd sites. The maxima of the wave functions at even and odd sites are shifted relative to each other by $2\Delta_{el}$.

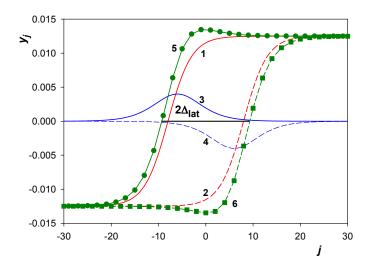The wave function must also be brought to a continual limit. The envelope of this wave

340

Fig. 4. Approximation of actual deviations from equilibrium positions y_j (circles for odd sites and squares for even sites) by the sum of two analytical dependences. $2\Delta_{\text{lat}}$ – distance between tangential dependencies for even and odd nodes.
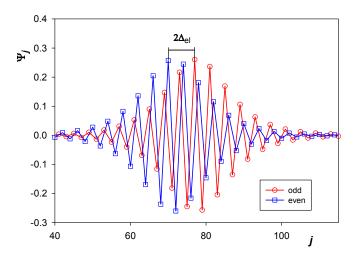

Fig. 5. Polaron wave function. Circles – odd sites, squares – even sites.

function can be represented as:

$$\Theta(\xi, t) = \frac{B}{\cosh[d(\xi - v_{\text{p}}t)]}, \tag{12}$$

where B is the amplitude and d is the width parameter. The continual function $\Theta(\xi, t)$ is related to the discrete wave function by relations:

$$
\begin{aligned}
\Psi_{2j-1} &= (-1)^j \exp(i\phi_{2j-1})\Theta[(2j-1)r_{\text{av}} - \Delta_{\text{el}}]; \\
\Psi_{2j} &= (-1)^{j-1} \exp(i\phi_{2j})\Theta[2jr_{\text{av}} + \Delta_{\text{el}}].
\end{aligned}
\tag{13}
$$

Here, factors of the type $(-1)^j$ transform the sign-alternating function Ψ into a smooth function, and the factors $\exp(i\phi_j)$ transform the component of the complex function at the j- th site to the real value for the Θ function.

341

The values of the introduced parameters depend on the polaron speed (Fig. 3) and will be determined as a result of the analytical solution.

Comparison of analytical and numerical calculations

This section will compare the parameters of the problem, which are determined numerically and analytically. These parameters are compared at different polaron speeds. Figure 6 shows the comparison of parameters A_1 and Δ_{lat}.
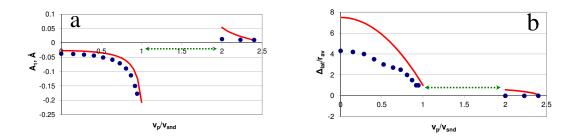

Fig. 6. Polaron parameters (A_1 panel a, and Δ_{lat} panel b) vs polaron speed. Analytical solution of the continuum model (lines); MD numerical simulations of the OE model (filled circles). The range of forbidden speedss is shown by dotted two-headed arrow on each panel.

Despite some quantitative difference, the agreement is quite satisfactory. Most importantly, the analytical solution correctly describes the forbidden energy range for a supersonic polaron: the analytical solution for A_1 diverges at both boundaries of the forbidden speed range.

Dynamic stability of a polaron on a lattice

The initial conditions for a freely moving polaron are determined from the analytical solution. Coordinates are determined directly from analytical expressions (25) with inverse replacement to discrete coordinates. The parameters are calculated from the solutions of the systems of algebraic equations (27) and (28) for a subsonic and supersonic polaron, respectively. The discrete wave function is defined similarly. The speeds are calculated by time differentiation of the expressions for the coordinates.

Figure 7 shows the evolution of a subsonic and supersonic polaron on large time scales. A subsonic polaron moves steadily at a constant speed over the entire time range. The dynamics of a supersonic polaron is very different. The polaron begins to move at a speed of $v_{ini} = 2.5 v_{snd}$ and slowly loses speed until, at $t \approx 6\,000$ fs, this speed reaches the upper limit of the forbidden speed range. After that, the polaron loses speed very quickly. Moreover, the stationary speed of the polaron becomes weakly negative.

The difference in the dynamics of sub- and supersonic polarons can be explained as follows. A subsonic polaron does not generate any additional lattice perturbations during its motion. Any disturbances propagate with speeds of sound exceeding the speed of a polaron, and excitations have time to completely relax. Therefore, the dynamics of the subsonic polaron is stable.

Although there is an analytical solution for a supersonic polaron, it is obtained in the continuum limit. The lattice discreteness and the complex profile of the polaron shape and wave function call into question the validity of the continuum approximation for a supersonic polaron. Nevertheless, a supersonic polaron travels a fairly large distance ($\sim 1\,000$) of lattice sites. This indicates a fairly successful analytical approximation.
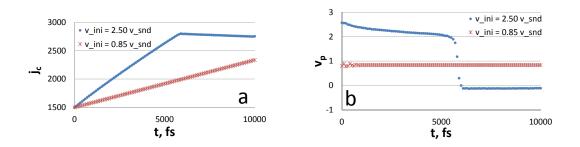
Fig. 7. Polaron center (**a**) and polaron speed (**b**) vs time for subsonic polaron with an initial speed $0.85v_{\text{snd}}$ (asterisks) and supersonic polaron with initial speed $2.5v_{\text{snd}}$ (filled circles).

A possible explanation for the stop of the polaron could be as follows. The shape of the polaron undergoes strong changes in the transition from subsonic to supersonic polaron (compare panels (e) and (f) in Fig. 3). The contribution of the local deformation of the lattice $\sim A_2 \cosh^{-2}[d(\xi - vt)]$ increases. But more importantly, the sign of the hyperbolic tangent changes, which indicates the appearance of lattice deformation in the polaron region. Thus, the motion of a supersonic polaron is accompanied by the generation of excitations. These excitations move at the speed of sound and remain behind the polaron. Stresses accumulate in the lattice and a critical state is reached when the motion of the polaron becomes unfavorable. Of the two possible scenarios – the destruction of the polaron and its stopping – the last one is realized. At the moment of stopping, the momentum of the polaron is transferred to the lattice. This issue requires additional research.

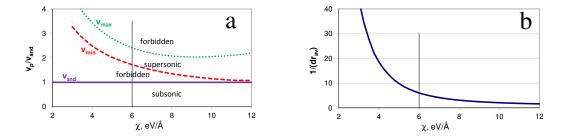**Influence of parameters on the dynamics of a polaron**

Fig. 8. Analytical solution: the maximum (dotted line) and minimum (dashed line) supersonic polaron speeds vs χ (**a**); the half-width of the polaron moving at v_{max} vs χ (**b**). The vertical thin lines in both panels indicate the χ value used in the above numerical simulations.

The analytical solution allows predicting the dependence of the polaron properties on the model parameters (bond rigidities, electron-phonon interaction, etc). For example, one can trace how the value of the parameter of the electron-phonon interaction affects the range of allowed polaron speeds. Figure 8,b shows the dependence of the polaron width $1/(dr_{\text{av}})$ on the parameter of electron-phonone interaction ξ. The polaron width increases with decreasing ξ. This leads to

343

the fact that the region of forbidden supersonic speeds changes together with the parameter ξ, (this region lies below the $v_{\min}$ curve and above the $v_{\max}$ curve in Figure 8,a.

CONCLUSIONS

The main output of this work is twofold. First, an efficient one-electron model is proposed for a dimerized PA lattice with free boundary conditions. This model allows calculations of the polaron dynamics at large time scales and lattice lengths (up to 10^4 sites). This makes it possible to find out the stability of the polaron and its stationary characteristics. It was found that the subsonic polaron is very stable. A supersonic polaron evolves in such a way that at first it slowly decreases its speed to values, corresponding to the lower limit of forbidden speeds, and then it stops very abruptly and starts slow motion in the opposite direction. A possible explanation is that as it moves at supersonic speed, deformations build up in the lattice. The reason is the dramatic difference between the shapes of sub- and supersonic polarons. This is especially true for the change in the sign of the hyper-tangential envelope, which means different degrees of deformation of the lattice in the asymptotics. Stopping the polaron means that the polaron has lost momentum and, according to the conservation law, should emit forward a wave packet of vibrational perturbations. This issue is supposed to be studied in more detail in the next work.

Second, the proposed OE model makes it possible to formulate a continual approximation for the problem of the polaron dynamics in the absence of an electric field. It was previously known that in an electric field a polaron can move at stationary speeds slightly less than the speed of sound and at supersonic speeds. Moreover, there is a range of forbidden speeds for a supersonic polaron. It turned out that the same laws are true for a freely moving polaron. Therefore, the continual model is a useful tool for studying all aspects of polaron dynamics.

The continual model, formulated in the form of partial differential equations, has a solution containing parameters. The values of these parameters are calculated from a system of algebraic equations in terms of the polaron speed. Due to the fact that the shapes of the sub- and supersonic polarons are different and also different is the system of these equations for both types of polarons. It follows from the solutions of these equations that they diverge at both boundaries of the forbidden speed range. This manifests itself in such a distortion of the polaron shape that it becomes incompatible with the lattice geometry.

The analytical solution makes it possible to find out the influence of the parameters of the problem on the properties of the polaron. In particular, the analytics predicts a decrease of the gap between subsonic and supersonic speeds with an increase in the electron-phonon interaction, accompanied by a decrease in the polaron width. With a sufficiently large electron-phonon interaction, when the width of the polarons becomes about several lattice sites, the gap disappears.

The obtained analytical solution makes it possible to better understand the laws governing the dynamics of a polaron in an electric field. Although there are questions that require further study. For example, the reasons why the speed of a polaron in an electric field changes from subsonic to supersonic in a very small ($\sim 10^{-4}$ meV/Å) range of electric field strengths are still unclear.

APPENDIX. CONTINUUM APPROXIMATION FOR POLARON

The partial differential equations are constructed on the base of equations of motion for the lattice displacements $x_j(t)$ (6) and the electron wave function $\Psi_j(t)$ (7). The wave function is assumed to be a lattice-modulated plane wave, i.e. it has the following form:

$$\Psi_j(t) = \exp\left[-\mathrm{i}(\omega t - kj)\right]\psi_j(t), \tag{14}$$

where $k \ll 1$, ψ_j are real, and the signs of ψ_j are chosen that $\chi\psi_{2j-1}\psi_{2j} \geq 0$ and $\chi\psi_{2j}\psi_{2j+1} \leq 0$. The sign alternation is inherent to the wave function of the $(N/2+1)$-th eigenfunction.

The following change of variables

$$\begin{aligned}
\psi_{2j-1} &= (-1)^{j-1}\phi_{2j-1} \\
\psi_{2j} &= (-1)^{j-1}\phi_{2j}
\end{aligned} \tag{15}$$

results in a smooth variable ϕ_j. Using variables y_j and ϕ_j, Eqs. (6) transform into

$$M\ddot{y}_{2j-1} = 2k_0(y_{2j} + y_{2j-2} - 2y_{2j-1}) - \Delta(y_{2j} - y_{2j-2}) + 2\chi\left[\phi_{2j-1}\phi_{2j} + \phi_{2j-2}\phi_{2j-1}\right];$$

$$M\ddot{y}_{2j} = 2k_0(y_{2j+1} + y_{2j-1} - 2y_{2j}) + \Delta(y_{2j+1} - y_{2j-1}) - 2\chi\left[\phi_{2j}\phi_{2j+1} + \phi_{2j-1}\phi_{2j}\right], \tag{16}$$

where $k_0 = (K_d + K_s)/4$ and $\Delta = (K_d - K_s)/2$ are introduced for bravity.

Next it is necessary to separate the variables related to different odd and even sublattices. For this, the following change of variables is made:

$$\begin{aligned}
y_{2j-1} &= v_{2j-1}; \quad y_{2j} = u_{2j}; \\
\phi_{2j-1} &= \mho_{2j-1}; \quad \phi_{2j} = \Omega_{2j}.
\end{aligned} \tag{17}$$

The result is:

$$M\ddot{v}(\xi, t) = 2k_0\left[u(\xi + r_{av}, t) + u(\xi - r_{av}, t)\right] - 4k_0 v(\xi, t) - \Delta\left[u(\xi + r_{av}, t) - u(\xi - r_{av}, t)\right] \\ + 2\chi\mho(\xi, t)\left[\Omega(\xi + r_{av}, t) + \Omega(\xi - r_{av}, t)\right];$$

$$M\ddot{u}(\xi, t) = 2k_0\left[v(\xi + r_{av}, t) + v(\xi - r_{av}, t)\right] - 4k_0 u(\xi, t) + \Delta\left[v(\xi + r_{av}, t) - v(\xi - r_{av}, t)\right] \\ - 2\chi\Omega(\xi, t)\left[\mho(\xi + r_{av}, t) + \mho(\xi - r_{av}, t)\right], \tag{18}$$

where ξ is a continuum variable. Then we make another change of variables in the following form:

$$\begin{aligned}
v(\xi, t) &= p(\xi - \Delta_{lat}, t) + q(\xi - \Delta_{lat}, t); \\
u(\xi, t) &= p(\xi + \Delta_{lat}, t) - q(\xi + \Delta_{lat}, t); \\
\mho(\xi, t) &= \Theta(\xi - \Delta_{el}, t); \\
\Omega(\xi, t) &= \Theta(\xi + \Delta_{el}, t).
\end{aligned} \tag{19}$$

Here, the relative shift of sublattices is explicitly taken into account through parameters Δ_{lat} and Δ_{el}. These equations are expanded into the Taylor series upto the second order. Then the system of partial differential equations follows:

$$\begin{aligned}
M\ddot{p} &= -c_1 q' + c_2 p'' + 8\chi\Delta_{lat}\Theta\Theta'; \\
M\ddot{q} &= -8k_0 q + c_1 p' - c_2 q'' + 2\chi\left[2\Theta^2 + 2(\Delta_{lat}^2 - \Delta_{el}^2)(\Theta')^2 + (2\Delta_{lat}^2 + 2\Delta_{el}^2 + r_{av}^2)\Theta\Theta''\right],
\end{aligned} \tag{20}$$

where

$$c_1 = 8k_0\Delta_{\text{lat}} - 2\Delta r_{\text{av}};$$
$$c_2 = 2k_0(4\Delta_{\text{lat}}^2 + r_{\text{av}}^2) - 4\Delta\Delta_{\text{lat}}r_{\text{av}}. \tag{21}$$

The continuous differential equation derived from Eqs. (7) is obtained similarly using the change of variables (10), (14), (15), (17) and (19). The equation is written for the variable $\Phi(\xi, t)$:

$$\Phi(\xi, t) = \exp\left[-\mathrm{i}(\omega t - k\xi)\right]\Theta(\xi, t) \tag{22}$$

and

$$\mathrm{i}\overline{h}\dot{\Phi} = 2\chi\delta\Phi - \beta\Phi'' - 4\chi q\Phi + 4\chi\Delta_{\text{lat}}p'\Phi, \tag{23}$$

where $\beta = 4t_0\Delta_{\text{el}}r_{\text{av}} - \chi\delta(4\Delta_{\text{el}}^2 + r_{\text{av}}^2)$. Thus we get the system of the continuum partial differential equations

$$M\ddot{p} = -c_1q' + c_2p'' + 8\chi\Delta_{\text{lat}}\Theta\Theta';$$
$$M\ddot{q} = -8k_0q + c_1p' - c_2q'' + 2\chi\left[2\Theta^2 + 2(\Delta_{\text{lat}}^2 - \Delta_{\text{el}}^2)(\Theta')^2 + (2\Delta_{\text{lat}}^2 + 2\Delta_{\text{el}}^2 + r_{\text{av}}^2)\Theta\Theta''\right];$$
$$\mathrm{i}\overline{h}\dot{\Phi} = 2\chi\delta\Phi - \beta\Phi'' - 4\chi q\Phi + 4\chi\Delta_{\text{lat}}p'\Phi. \tag{24}$$

The system has a particular solution in the following form:

$$p(\xi, t) = A_1\tanh\left[d(\xi - v_{\text{p}}t)\right];$$
$$q(\xi, t) = \frac{A_2}{\cosh^2\left[d(\xi - v_{\text{p}}t)\right]}; \tag{25}$$
$$\Theta(\xi, t) = \frac{B}{\cosh\left[d(\xi - v_{\text{p}}t)\right]}.$$

To get a solution in the original coordinates $\{x_j, \Psi_j\}$, the backward variable changes should be maid: $\{p, q, \Theta, \Phi\} \xrightarrow{(22),(19)} \{v, u, \text{\O}, \Omega\} \xrightarrow{(17),(15)} \{y, \psi\} \xrightarrow{(10),(14)} \{x, \Psi\}$.

The polaron parameters $A_1, A_2, d, \Delta_{\text{lat}}, \Delta_{\text{el}}, B, \omega, k$ are defined through the polaron speeds v_p. This relationship is obtained from the substitution (25) into the system (20–23) taking into account the normalization of the wave function:

$$\int_{-\infty}^{\infty}\Theta^2(\xi, t)\,\mathrm{d}\xi = 1. \tag{26}$$

Subsonic and supersonic polarons are considered separately. The relation between parameters for the subsonic polaron is the system of algebraic equations:

$$\left[(8\Delta_{\text{lat}}^2 + 2r_{\text{av}}^2)k_0 - 4\Delta r_{\text{av}}\Delta_{\text{lat}} - Mv^2\right]A_1 + 2\chi\Delta_{\text{lat}} = 0;$$
$$\left[4k_0\Delta_{\text{lat}} - \Delta r_{\text{av}}\right]A_1 + \chi = 0;$$
$$2\chi\delta\Delta_{\text{el}} - t_0r_{\text{av}} = 0;$$
$$\beta d + 2\chi\Delta_{\text{lat}}A_1 = 0; \tag{27}$$
$$d - 2B^2 = 0;$$
$$\overline{h}v - 2\beta k = 0;$$
$$\overline{h}\omega - 2\chi\delta + \beta d^2 = 0.$$

Here we put parameters $k = A_2 = 0$ because of there smallness. The system is obtained by substituting (25) into (20, 23) and equating to zero the coefficients in front of terms:

$\cosh^{-2}\left[d(\xi - vt)\right]$, $\cosh^{-4}\left[d(\xi - vt)\right]$ and $\sinh\left[d(\xi - vt)\right]\cosh^{-3}\left[d(\xi - vt)\right]$.

The algebraic system for the supersonic polarons is obtained in a similar way:

$$
\begin{aligned}
&\left[(8\Delta_{\text{lat}}^2 + 2r_{\text{av}}^2)k_0 - 4\Delta r_{\text{av}}\Delta_{\text{lat}} - Mv^2\right]dA_1 - \left[8k_0\Delta_{\text{lat}} - 2\Delta r_{\text{av}}\right]A_2 + 2\chi\Delta_{\text{lat}}d = 0; \\
&4k_0A_2 + 2\left[(8\Delta_{\text{lat}}^2 + 2r_{\text{av}}^2)k_0 - 4\Delta r_{\text{av}}\Delta_{\text{lat}} + Mv^2\right]d^2A_2 - \chi d = 0; \\
&3\left[(8\Delta_{\text{lat}}^2 + 2r_{\text{av}}^2)k_0 - 4\Delta r_{\text{av}}\Delta_{\text{lat}} + Mv^2\right]A_2 - \chi(3\Delta_{\text{lat}}^2 + \Delta_{\text{el}}^2 + r_{\text{av}}^2)d = 0; \\
&2\chi\delta\Delta_{\text{el}} - t_0 r_{\text{av}} = 0; \\
&\beta d^2 + 2\chi\Delta_{\text{lat}}dA_1 - 2\chi A_2 = 0; \\
&d - 2B^2 = 0; \\
&\overline{h}v - 2\beta k = 0; \\
&\overline{h}\omega - 2\chi\delta + \beta d^2 = 0.
\end{aligned}
\tag{28}
$$

The algebraic systems (27) and (28) implicitly determines the dependences of the polaron parameters on its speed. Despite the awkwardness, they are easily solved numerically.

REFERENCES

1. Kausar A. Review on structure, properties and appliance of essential conjugated polymers. *American Journal of Polymer Science & Engineering.* 2016. V. 4. P. 91–102.

2. Ziadan K.M. Conducting Polymers Application. In: *New Polymers for Special Applications.* Ed. Ailton De Souza Gomes. Brazil: Federal University of Rio de Janeiro, 2012. doi: 10.5772/3345

3. Ravichandran R., Sundarrajan S., Venugopal J.R., Mukherjee Sh., Ramakrishna S. Applications of conducting polymers and their issues in biomedical engineering. *J. R. Soc. Interface.* 2010. V. 7. P. S559. doi: 10.1098/rsif.2010.0120.focus

4. Heeger A.J. Nobel Lecture: Semiconducting and metallic polymers: The fourth generation of polymeric materials. *Rev. Mod. Phys.* 2001. V. 73. P. 681. doi: 10.1103/RevModPhys.73.681

5. MacDiarmid A.G. Nobel Lecture "Synthetic metals": A novel role for organic polymers. *Rev. Mod. Phys.* 2001. V. 73. P. 707. doi: 10.1103/RevModPhys.73.701

6. Shirakawa H. Nobel Lecture: The discovery of polyacetylene film – the dawning of an era of conducting polymers. *Rev. Mod. Phys.* 2001. V. 73. P. 713. doi: 10.1103/RevModPhys.73.713

7. Lu N., Li L., Geng D., Liu M. A review for polaron dependent charge transport in organic semiconductor. *Organic Electronics.* 2018. V. 61. P. 223. doi: 10.1016/j.orgel.2018.05.053

8. Su W.P., Schrieffer J.R., Heeger A.J. Solitons in polyacetylene. *Phys. Rev. Lett.* 1979. V. 42. P. 1698. doi: 10.1103/PhysRevLett.42.1698

9. Su W.P., Schrieffer J.R., Heeger A.J. Soliton excitations in polyacetylene. *Phys. Rev. B.* 1980. V. 22. P. 2099. doi: 10.1103/PhysRevB.22.2099

10. Meier E.J., An F.A., Gadway B. Observation of the topological soliton state in the Su-Schrieffer-Heeger model. *Nat. Commun.* 2016. V. 7. P. 13986. doi: 10.1038/ncomms13986

11. Fathizadeh S., Behnia S. Charge and spin dynamics in DNA nanomolecules: Modeling and applications. In: *21st Century Nanoscience — A Handbook Bioinspired Systems and Methods. V. 7.* Ed. Sattler K.D. Boca Raton: CRC Press, 2020. P. 12.

12. Terai A., Ono Y. Phonons around a soliton and a solaron in Su-Schrieffer-Heeger's model of trans-(CH)$_x$. *J. Phys. Soc. Japan.* 1986. V. 55. P. 213. doi: 10.1143/JPSJ.55.213

13. Ono Y., Terai A. Motion of charged soliton in polyacetylene due to electric field. *J. Phys. Soc. Japan.* 1990. V. 59. P. 2893. doi: 10.1143/JPSJ.59.2893

14. Rakhmanova S.V., Conwell E.M. Nonlinear dynamics of an added carrier in trans-polyacetylene in the presence of an electric field. *Synthetic Metals.* 2000. V. 110. P. 37. doi: 10.1016/S0379-6779(99)00261-1

15. Johansson A.A., Stafström S. Soliton and polaron transport in trans-polyacetylene. *Phys. Rev. B.* 2002. V. 65. P. 045207. doi: 10.1103/PhysRevB.65.045207

16. Johansson A.A., Stafström S. Nonadiabatic simulations of polaron dynamics. *Phys. Rev. B.* 2004. V. 69. P. 235205. doi: 10.1103/PhysRevB.69.235205

17. e Silva G.M. Electric-field effects on the competition between polarons and bipolarons in conjugated polymers. *Phys. Rev. B.* 2000. V. 61. P. 10777. doi: 10.1103/PhysRevB.61.10777

18. Roncaratti L.F., Gargano R., e Silva G.M. Theoretical temperature dependence of the charge-carrier mobility in semiconducting polymers. *J. Phys. Chem. A.* 2009. V. 113. P. 14591. doi: 10.1021/jp9041759

19. Ribeiro L.A., de Brito S.S., de Oliveira Neto P.H. Trap-assisted charge transport at conjugated polymer interfaces. *Chem. Phys. Lett.* 2016. V. 644. P. 121. doi: 10.1016/j.cplett.2015.12.006

20. Sun S., Zhang Y., Liu X., An Z. Spectral analysis of polaron dynamics in conjugated polymers. *Phys. Chem. C.* 2019. V. 123. P. 28569. doi: 10.1021/acs.jpcc.9b07330

21. Liu X.J., Gao K., Fu J.Y., Li Y., Wei J.H., Xie S.J. Effect of the electric field mode on the dynamic process of a polaron. *Phys. Rev. B.* 2006. V. 74. P. 172301. doi: 10.1103/PhysRevB.74.172301

22. Ribeiro L.A. , da Cunha W.F., de Oliveria Neto P.H., Gargano R., e Silva G.M. Effects of temperature and electric field induced phase transitions on the dynamics of polarons and bipolarons. *New J. Chem.* 2013. V. 37. P. 2829–2836. doi: 10.1039/C3NJ00602F

23. da Silva M.V.A., de Oliveira Neto P.H., da Cunha W.F., Gargano R., e Silva G.M. Supersonic quasi-particles dynamics in organic semiconductors. *Chem. Phys. Let.* 2012. V. 550. P. 146. doi: 10.1016/j.cplett.2012.09.012

24. Astakhova T., Vinogradov G. New aspects of polaron dynamics in electric field. *Eur. Phys. J. B.* 2019. V. 92. P. 247. doi: 10.1140/epjb/e2019-100339-y

25. Korshunova A.N., Lakhno V.D. Various regimes of charge transfer in a Holstein chain in a constant electric field depending on its intensity and the initial charge distribution. *Math. Biology and Bioinformatics*. 2018. V. 7. Article No. e4. doi: 10.17537/icmbb18.89

26. Chetverikov A.P., Ebeling W., Lakhno V.D., Shigaev A.S., Velarde M.G. On the possibility that local mechanical forcing permits directionally-controlled long-range electron transfer along DNA-like molecular wires with no need of an external electric field. Mechanical control of electrons. *Eur. Phys. J. B.* 2016. V. 89. P. 101. doi: 10.1140/epjb/e2016-60949-1

27. Astakhova T., Vinogradov G. Single-electron model for polaron on dimerized lattice. *Math. Biol. Bioinf.* 2019. V. 14. P. 625. doi: 10.17537/2019.14.625

28. Astakhova T., Vinogradov G. Subsonic and supersonic polarons in one-electron model of polyacetylene. *Eur. Phys. J. B.* 2020. V. 93. P. 127. doi: 10.1140/epjb/e2020-10113-7

29. Astakhova T.Yu., Vinogradov G.A., Kashin V.A. Polaron in an electric field as a generator of coherent lattice vibrations. *Rus. J. Phys. Chem. B*. 2018. V. 12. No. 6. P. 1. doi: 10.1134/S1990793118050147